# **Investigation of Nanosponge Based Delivery of Rutin and Brucine for Cancer Therapy**

Pallavi Sardana<sup>1</sup>, Anroop B Nair<sup>2,\*</sup>, Sweta Dalal<sup>1,3,4</sup>, Mani Shankar Bhattacharyya<sup>3,4</sup>, Shery Jacob<sup>5</sup>, Mohamed A Morsy<sup>2</sup>, Katharigatta N Venugopala<sup>2</sup>, Mahesh Attimarad<sup>2</sup>, Tamer M Shehata<sup>2</sup>, Rekha Rao<sup>1,\*</sup>

#### **ABSTRACT**

**Background:** Both rutin and brucine can suppress tumor growth mainly through the induction of apoptosis. This study aims to evaluate the potential of nanosponge based delivery to enhance the therapeutic efficacy of rutin and brucine combination against cancer. Materials and Methods: Rutin and brucine nanosponges were prepared separately by employing the quasi-emulsion solvent diffusion method. The formulations were examined for various pharmaceutical properties as well as antioxidant and cytotoxicity effects. Results: The prepared nanosponges resulted in higher drug encapsulation (81% and 88% for rutin and brucine, respectively). FTIR, DSC, and XRD confirm the successful entrapment of bioactives and amorphous dispersion without drug-excipient interactions. Scanning electron microscopy revealed spherical, non-aggregated particles with size range of 300-400 nm. In vitro release studies demonstrated sustained drug release from nanosponges compared to pure bioactives. The DPPH radical scavenging assay showed that combined delivery of nanosponges produced superior antioxidant activity, displaying a synergetic effect at lower concentrations (10-50 µg/mL). Notably, cytotoxic effect on HaCaT cell lines showed that the combination of delivery leads to ~4 fold improvement in potency with marked reduction in IC $_{so}$  (20.66  $\mu g/mL$ ) than individual administration. **Conclusion:** Combination administration using developed nanosponges led to a notable rise in antioxidant activity as well as enhanced anticancer activity, suggesting that this could be a viable strategy for cancer therapy.

**Keywords:** Antioxidant Activity, Brucine, Combination Therapy, Cytotoxicity, Nanosponges, Rutin.

#### **Correspondence:**

#### Prof. Dr. Anroop B Nair

Department of Pharmaceutical Sciences, College of Clinical Pharmacy, King Faisal University, Al-Ahsa 31982, SAUDI ARABIA. Email: anair@kfu.edu.sa

#### Dr. Rekha Rao

Department of Pharmaceutical Sciences, Guru Jambheshwar University of Science and Technology, Hisar-125001, Haryana, INDIA.

Email: rekhaline@gmail.com

**Received:** 09-06-2025; **Revised:** 18-08-2025; **Accepted:** 21-10-2025.

# **INTRODUCTION**

Cancer is a highly complex and multifactorial disease involving dysregulated signaling pathways that drive uncontrolled cellular proliferation, evasion of apoptosis, sustained angiogenesis, immune escape, and the ability to invade surrounding tissues and metastasize to distant organs. <sup>1,2</sup> In 2020, more than 19.3 million new cancer cases were diagnosed worldwide, resulting in approximately 10 million deaths. <sup>3</sup> Incidence rates are projected to rise further due to aging populations, environmental risk factors, and lifestyle-related determinants. Current cancer treatments include surgery, radiation, chemotherapy, immunotherapy, and

ASSOCIATION OF THE PROPERTY OF

**DOI:** 10.5530/ijper.20263680

#### Copyright Information:

Copyright Author (s) 2026 Distributed under Creative Commons CC-BY 4.0

Publishing Partner: Manuscript Technomedia. [www.mstechnomedia.com]

targeted therapies, often used in multimodal regimens.<sup>4</sup> Despite major advancements in diagnostic imaging, molecular profiling, and therapeutic strategies, conventional chemotherapy continues to represent a central component of cancer management. However, its clinical utility is significantly limited by inherent challenges, including non-specific biodistribution, dose-limiting systemic toxicities, emergence of multidrug resistance, and suboptimal pharmacokinetics that hinder effective drug accumulation at tumor sites.<sup>5,6</sup> These challenges have driven interest in combination approaches such as chemo-immunotherapy, as well as advanced delivery systems that aim to enhance tumor targeting, overcome resistance, and improve therapeutic outcomes.<sup>7,8</sup>

The co-delivery of chemotherapeutic agents with phytochemicals using nanocarriers has emerged as a promising strategy to overcome the limitations of conventional monotherapy. Phytochemicals such as curcumin, resveratrol, and quercetin exhibit pleiotropic anticancer effects, including modulation of

<sup>&</sup>lt;sup>1</sup>Department of Pharmaceutical Sciences, Guru Jambheshwar University of Science and Technology, Hisar, Haryana, INDIA.

<sup>&</sup>lt;sup>2</sup>Department of Pharmaceutical Sciences, College of Clinical Pharmacy, King Faisal University, Al-Ahsa, SAUDI ARABIA.

<sup>&</sup>lt;sup>3</sup>The Biochemical Engineering Research and Process Development Centre (BERPDC), CSIR- Institute of Microbial Technology (IMTECH), Chandigarh, INDIA.

<sup>&</sup>lt;sup>4</sup>Academy of Scientific and Innovative Research (AcSIR), Ghaziabad, Uttar Pradesh, INDIA.

<sup>&</sup>lt;sup>5</sup>Department of Pharmaceutical Sciences, College of Pharmacy, Gulf Medical University, Ajman, UNITED ARAB EMIRATES.

signaling pathways, induction of apoptosis, and reversal of MDR, thereby sensitizing tumor cells to standard chemotherapeutics. 9,10 The combination of natural phytochemicals with conventional chemotherapeutic agents has attracted significant attention, as their intrinsic antioxidant, pro-apoptotic, and anti-proliferative activities can potentiate the anticancer efficacy of synthetic drugs while concurrently reducing treatment-associated toxicity. Nanocarrier-based co-delivery systems, including vesicular carriers such as liposomes and niosomes, as well as lipid-based platforms like solid lipid nanoparticles, nanostructured lipid carriers, and polymeric micelles, facilitate synchronized drug release, enhance tumor-specific targeting, and minimize systemic toxicity, thereby improving therapeutic efficacy compared to free drug combinations. 12-14

Among these systems, nanosponges have recently gained significant attention due to their highly porous, cross-linked polymeric architecture, which allows high drug loading, controlled release, and protection of labile phytochemicals from degradation.<sup>15</sup> Nanosponge-based formulations are capable to enhance the solubility and bioavailability of hydrophobic phytochemicals as well as permit the simultaneous incorporation of multiple drugs, making them particularly attractive for co-delivery strategies.<sup>16</sup> By modulating release kinetics, nanosponges achieve sustained drug delivery, maintaining therapeutic plasma concentrations over extended periods and reducing dosing frequency.<sup>17</sup> A cyclodextrin nanosponge based hydrogel was successfully developed for the co-delivery of curcumin and resveratrol.<sup>18</sup> The system enhanced drug release, photostability, and showed strong synergistic cytotoxicity against MCF-7 breast cancer cells. Peptide-functionalized nanosponges have been developed for the co-delivery of paclitaxel and camptothecin, where tumor-targeting peptides improved selectivity and significantly reduced tumor growth in an in vivo lung cancer model.19 pH-sensitive and ligand-functionalized nanosponges enable controlled, targeted co-delivery of anticancer agents, while theranostic nanosponges incorporating imaging probes allow simultaneous treatment and real time monitoring, showing enhanced efficacy in cancer models.<sup>20</sup> Collectively, nanosponge mediated co-delivery platforms offer a versatile and effective approach to maximize the therapeutic potential of phytochemical-chemotherapy combinations.<sup>21</sup>

Rutin, a naturally occurring flavonoid glycoside (quercetin-3-rutinoside), possesses strong antioxidant and anti-inflammatory properties, along with anticancer potential. It exerts its effects by modulating key signaling pathways such as PI3K/Akt, MAPK, and NF-κB, leading to cell cycle arrest and apoptosis in various cancers, including colon, breast, and lung malignancies.<sup>22</sup> Despite its promising pharmacological profile, rutin exhibits poor aqueous solubility, limited gastrointestinal permeability, and rapid metabolic degradation, resulting in low systemic bioavailability.<sup>23</sup>

Consequently, the design of advanced delivery systems is essential to improve its solubility, protect against premature degradation, and enable sustained therapeutic release.

Brucine is an indole alkaloid derived from Strychnos nux-vomica that exhibits notable anticancer activity through multiple mechanisms, including induction of apoptosis, inhibition of angiogenesis, and suppression of tumor cell proliferation. It has demonstrated efficacy against hepatocellular carcinoma, breast cancer, and lung cancer models, but its clinical use is limited by narrow therapeutic index and systemic toxicity.<sup>24</sup> Similar to many plant-derived alkaloids, brucine is limited by a narrow therapeutic index and significant systemic toxicity, notably neurotoxic and cardiotoxic effects, which restrict its clinical utility.<sup>25</sup> Therefore, the development of controlled-release delivery strategies is critical to utilize its anticancer potential while improving safety. In this context, the development of nanosponges can improve drug loading and provide controlled release of both rutin and brucine while protecting these biactives from premature degradation, and improve their therapeutic efficacy in anticancer applications.

Although rutin and brucine have been individually investigated for their anticancer potential, their combined delivery via nanosponge carriers remains largely unexplored. To address this gap, the present study focuses on the development and characterization of rutin and brucine loaded nanosponges for combination cancer therapy. This approach aims to establish nanosponge based combination delivery as a strategy to enhance the therapeutic effectiveness of rutin and brucine while minimizing their individual pharmacokinetic and toxicity related limitations. The nanosponges were fabricated using ethyl cellulose as the polymeric matrix through a quasi-emulsion solvent diffusion method. Comprehensive characterization was performed by Scanning Electron Microscopy (SEM), Fourier Transform Infrared (FTIR) spectroscopy, Differential Scanning Calorimetry (DSC), and X-ray diffraction, alongside evaluations of encapsulation efficiency, in vitro drug release, antioxidant activity, and anticancer efficacy.

# MATERIALS AND METHODS

#### Chemicals

Both bioactives, brucine and rutin, as well as sodium chloride, disodium hydrogen orthophosphate, and potassium dihydrogen phosphate, were purchased from High Purity Laboratory Chemicals, Mumbai, India. Ethyl cellulose and Polyvinyl Alcohol (PVA) were procured from Thomas Baker (chemicals), Mumbai, India. Dichloromethane (DCM) and methanol were brought from Loba Chemie, Mumbai, India, and Sisco Research Laboratories, Mumbai, India, respectively. HaCaT cell line was acquired from the National Centre for Cell Sciences, Pune, India. Distilled water was used for experimental studies.

#### **Estimation of Rutin and Brucine**

Stock solutions of rutin and brucine (100 µg/mL in methanol/phosphate buffer saline -PBS pH 7.4) were individually scanned in a Genesys UV-visible spectrophotometer (Thermo Fisher Scientific, Madison, USA) within the 200 to 800 nm range using the respective solvent as blank. The wavelengths corresponding to maximum absorbance were identified (357 nm for rutin and 265 nm for brucine). The isobestic point is determined from the recorded spectrum, which is the wavelength at which the spectra of two drugs intersect each other and was noted at 320 nm. For simultaneous estimation in binary mixtures, absorbance was recorded at the respective  $\lambda_{\rm max}$  and the isobestic wavelength, and drug concentrations were calculated using the isobestic point method based on the Beer-Lambert law.

# Preparation of Rutin and Brucine Loaded Nanosponges

Rutin and brucine encapsulated nanosponges were fabricated employing the quasi-emulsion solvent diffusion method reported previously with minor modifications.<sup>26,27</sup> The composition of prepared nanosponges is presented in Table 1. Briefly, a measured quantity of ethyl cellulose (500, 700, or 900 mg) was dissolved in 20 mL of DCM (internal organic phase) under magnetic stirring to get a clear solution. The respective drug (rutin or brucine) was added (100 mg) to this solution and stirred until completely dissolved. Separately, the external aqueous phase was prepared by dissolving PVA (20 mL) in distilled water, followed by heating (up to 70°C) with constant stirring until a clear solution was obtained. The prepared solution was cooled to room temperature. Then the organic phase was added dropwise to the aqueous phase while stirring at 500 rpm for 3 hr, resulting in nanosponges formation. Later, nanosponges were filtered using Whatman filter paper, rinsed with distilled water and then dried at 40°C in an oven.

#### **Production Yield**

The production yield of prepared nanosponges was calculated by comparing the practical yield with the theoretical yield. The practical yield was obtained by measuring the dried weight of bioactive loaded nanosponges after preparation. The theoretical weight was calculated as the total weight of drug and excipients used. The following formula was used to calculate the production yield.<sup>28</sup>

$$\% Production\ yield = \frac{Practical\ yield}{Theoretical\ yield} \times 100$$

#### **Encapsulation Efficiency**

Bioactives containing nanosponges were accurately weighed (20 mg) and grinded using a mortar and pestle. Methanol (10 mL) was added to the triturate and the mixture was sonicated in a bath sonicator for 15 min for complete release of encapsulated bioactive from nanosponges. The samples were filtered using 0.45  $\mu m$  pore size membrane filter and analyzed using UV spectrophotometer

(Thermo Fisher Scientific, Madison, USA). The following formula was used to calculate entrapment efficiency.<sup>29</sup>

%Entrapment Efficiency = 
$$\begin{cases} \frac{\text{Cr} \times \frac{Vr}{Mmp}}{Md(Md + Mp)} \end{cases} \times 100$$

Where Cr is the concentration of bioactive in the release medium, Vr is the volume of release medium, Mmp is the mass of porous nanosponges, and Md and Mp are the initial mass of the polymer and the drug/bioactive encapsulated, respectively.

## **FTIR Analysis**

FTIR spectra of blank, rutin loaded, and brucine loaded nanosponges were recorded using an FTIR spectrometer (Model BX-II, PerkinElmer, Waltham, MA, USA). Samples were prepared by the KBr disc method, in which the sample was mixed with spectroscopic-grade KBr and compressed at a pressure of 5 tons for 4 min using a hydraulic press. The spectra were recorded in the range of 400-4000 cm<sup>-1</sup> with a resolution of 2 cm<sup>-1</sup> at room temperature.<sup>28</sup>

# Field Emission-SEM (FE-SEM)

The surface topography and morphology of blank, rutin loaded, and brucine loaded nanosponges were examined using a FE-SEM instrument (Model 7610F Plus, JEOL, Peabody, MA, USA). Samples were sputter-coated with gold-palladium in an argon atmosphere at room temperature for 15-20 min to enhance conductivity.<sup>30</sup> Samples were observed under an accelerating voltage of 30 kV and images were captured at magnifications ranging from 10× to 300,000×.

#### **DSC Study**

Thermal analysis of blank nanosponges, and rutin plus brucine nanosponges combination (1:1 w/w) was performed using a DSC instrument (Discovery 25, TA InstrumentsWaters, New Castle, DE, USA) to investigate possible drug-polymer interactions and changes in crystallinity. Approximately 3-5 mg of each sample was accurately weighed and hermetically sealed in standard aluminum pans to prevent moisture loss and oxidation. An empty aluminum pan was used as a reference. The samples were heated from 10 to 300°C at a constant heating rate of 10°C/min under a continuous flow of nitrogen gas (50 mL/min) to provide an inert atmosphere and the DSC curves were recorded.

## X-ray Diffraction

X-ray diffraction patterns of blank, rutin loaded nanosponges, and brucine loaded nanosponges were recorded using a powder X-ray diffractometer (SmartLab 3 kW, Rigaku, UK). The diffraction profiles were obtained over a  $2\theta$  range of  $10^{\circ}$ - $80^{\circ}$ , with a step time of 0.5 s.<sup>28</sup> The total acquisition time for each sample was approximately 1 hr.

#### In vitro Release

The release profiles of pure bioactives, rutin loaded nanosponges, and brucine loaded nanosponges were evaluated using the dialysis bag method. Regenerated cellulose dialysis membranes (pore size 2.4 nm, MWCO 12,000-14,000 Da; Hi-Media Laboratories Pvt. Ltd., Mumbai, India) were pre-soaked overnight in PBS (pH 7.4). Accurately weighed samples (10 mg) were placed inside the dialysis bags, which were sealed at both ends with thread and immersed in 100 mL of PBS (pH 7.4) maintained at 37±0.5°C with constant stirring at 100 rpm. At predetermined time intervals, 2 mL aliquots were withdrawn and immediately replaced with an equal volume of fresh PBS. The drug concentration in each sample was quantified by UV spectrophotometry. Further, the data were analyzed using various mathematical models to determine release kinetics.<sup>31</sup>

# In vitro Anti-oxidant Activity

The antioxidant activity of pure rutin, pure brucine, rutin loaded nanosponges, brucine loaded nanosponges, and rutin plus brucine nanosponges (combination) was evaluated using a slightly modified 2,2-Diphenyl-1-Picrylhydrazyl (DPPH) assay based on the method described in the literature.<sup>32</sup> A 0.1 mM DPPH solution was prepared by dissolving 1.97 mg of DPPH in 50 mL of methanol. One milliliter of each test sample at different concentrations (10, 20, 50, 100, 200, 350, and 500 µg/ mL) was mixed with 1 mL of the DPPH solution. The mixtures were incubated in the dark at room temperature for 30 min, after which the absorbance was measured at 517 nm using a Genesys UV-visible spectrophotometer (Thermo Fisher Scientific, Madison, USA). A DPPH solution without any test sample served as the control, and methanol was used as the blank. A decrease in absorbance indicated increased free radical scavenging activity, which was calculated using the following equation:

Scavenging effect (%) 
$$= \left(\frac{A_{control} - A_{sample}}{A_{control}}\right) \times 100$$

Where,  $A_{control}$  is the absorbance of blank DPPH solution and  $A_{sample}$  is the absorbance of incubated sample.

# In vitro Cytotoxicity Assay Using HaCaT Cell Lines

The cytotoxicity of the test samples was evaluated using the 3-[4,5-dimethylthiazol-2-yl]-2,5 diphenyl tetrazolium bromide (MTT) assay. Briefly, in a 96-well plate, 10000 cells/well were seeded and grown for 24 hr at 37°C with 5%  $CO_2$  in an incubator. Then the media was replaced with 100  $\mu$ L of MTT with a concentration of 0.5 mg/mL and kept for 4 hr. Further, the MTT was removed and 100  $\mu$ L of DMSO was added to each well and kept for incubation at 37°C, 1 hr in dark conditions. The plates were gently agitated on a gyratory shaker to facilitate solubilization. Absorbance was measured at 570 nm with a reference wavelength of 630 nm using Agilent BioTek Synergy H1 Multimode Reader. % Cell viability was calculated based on the following formula. IC50 value was determined from the normalized best-fit cytotoxicity curve.

$$\% \ cell \ viability = \frac{\textit{Mean absorbance of treated cells}}{\textit{Mean absorbance of untreated cells}} \times 100$$

# **RESULTS AND DISCUSSION**

#### **Estimation of Rutin and Brucine**

Maximum absorbance wavelengths ( $\lambda_{max}$ ) of rutin and brucine were 357 nm and 265 nm, respectively. The overlay plot of both drugs is depicted in Figure 1. As observed from the figure, the isosbestic point, where the absorption spectra of both compounds intersect was determined to be 320 nm. The calibration curve was constructed for rutin and brucine in both methanol and PBS (pH 7.4), corresponding to their  $\lambda_{max}$  as well as at isobestic points. The graphs demonstrated that the concentrations of both drugs exhibited a linear relationship with absorbance, characterized by a regression coefficient, a slope and a Y-intercept (data not shown). The analytical method developed was found to be precise, specific, and robust.

# Preparation of Rutin and Brucine Loaded Nanosponges

The formulation of nanosponges was carried out by the quasi-emulsion solvent diffusion technique, which is widely used owing to its potential to produce porous, stable nanostructures with higher entrapment efficiency.<sup>33</sup> It has been described that adding the organic phase dropwise to the aqueous solution promotes fast diffusion of the organic solvent into the continuous

Batch	Rutin (mg)	Brucine (mg)	Ethyl cellulose (mg)	Polyvinyl alcohol (mg)	Dichloromethane (mL)
RUT-MIS-1	100	-	500	100	20
RUT-MIS-2	100	-	700	100	20
RUT-MIS-3	100	-	900	100	20
BRC-MIS-1	-	100	500	100	20
BRC-MIS-2	-	100	700	100	20
BRC-MIS-3	-	100	900	100	20

phase, resulting in polymer precipitation and trapping the drug inside a porous polymer matrix.<sup>34</sup> In addition, the formulation and stabilization of nanosponges are significantly influenced by the amount of PVA, ethyl cellulose (polymer) and solvent used. In this process, PVA functioned as an emulsifying agent to stabilize the formulation, while ethyl cellulose contributed to the structural framework of the nanosponges.<sup>33</sup>

Formulations were prepared by varying the drug to polymer ratios (1:5, 1:7 and 1:9) and evaluated for various properties. The production yield and encapsulation efficiency of the prepared batches are presented in Table 2. It can be seen that the increase in drug-to-polymer ratio from 1:5 to 1:7 increases the production yield and encapsulation efficiency in both cases. However, further increase in the ratio leads to decrease in both yield and encapsulation as seen in Table 2. The initial increase in drug entrapment could be explained by the fact that increasing polymer content often increases the accessible matrix for drug entrapment, in addition to increasing intramolecular forces, organic-phase viscosity, and slowing DCM diffusion. As a result, larger droplets and nanosponges with a denser polymer network will form, allowing for more bioactives to be encapsulated.<sup>29</sup> The decrease in drug entrapment at an increased ethyl cellulose ratio (1:9) could be attributed to a more viscous organic phase, which created larger droplets that solidified more slowly, allowing for greater drug partitioning into the aqueous phase.35 Batches RUT-MIS-2 and BRC-MIS-2 were chosen for further characterisation due to their higher drug encapsulation efficiency.

## **FTIR Analysis**

FTIR is an efficient technique for determining the functional groups in an unknown sample and predicting alterations to functional groups in any combination of substances. The FTIR spectra of blank, rutin loaded, and brucine loaded nanosponges are presented in Figure 2. A distinctive absorption peak at 3453 cm<sup>-1</sup> in the FTIR spectrum of blank nanosponges indicated the presence of hydroxyl (OH) groups of ethyl cellulose.<sup>36</sup> Bands at 2972 cm<sup>-1</sup> and 2874 cm<sup>-1</sup> indicate C-H stretching, which is typical for aliphatic hydrocarbons and indicates both intra and intermolecular hydrogen bonding in OH groups. The presence of PVA is confirmed by a distinct carbonyl band at 1738 cm<sup>-1</sup>, the band at 1636 cm<sup>-1</sup> corresponding to carbonyl (C=C) stretching, and the bands at 1445 cm<sup>-1</sup> and 1384.09 cm<sup>-1</sup> attributed to CH<sub>2</sub> bending vibration.<sup>37</sup> For rutin, the major drug peaks were observed at 3416 cm<sup>-1</sup> (O-H stretching), 2919 cm<sup>-1</sup> (aliphatic C-H), 1638 cm<sup>-1</sup> and 1618 cm<sup>-1</sup> (conjugated C=O/ C=C), and 1062 cm<sup>-1</sup> (strong sugar/ether bands), indicating drug

Table 2: Production yield and encapsulation efficiency of the prepared batches.

Batch	% Production yield	% Encapsulation efficiency
RUT-MIS-1	84%±0.014	57%±0.023
RUT-MIS-2	98%±0.021	81%±0.013
RUT-MIS-3	96%±0.011	76%±0.021
BRC-MIS-1	86%±0.019	59%±0.018
BRC-MIS-2	90%±0.011	88%±0.010
BRC-MIS-3	88%±0.016	80%±0.014

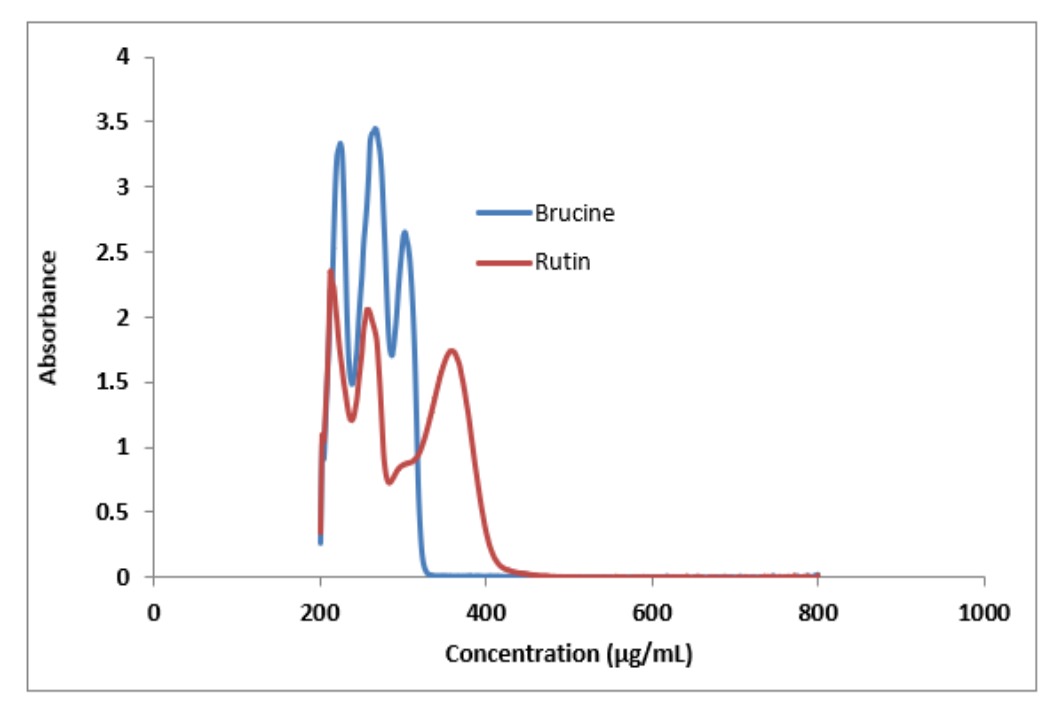


Figure 1: Overlay UV spectra of rutin and brucine.

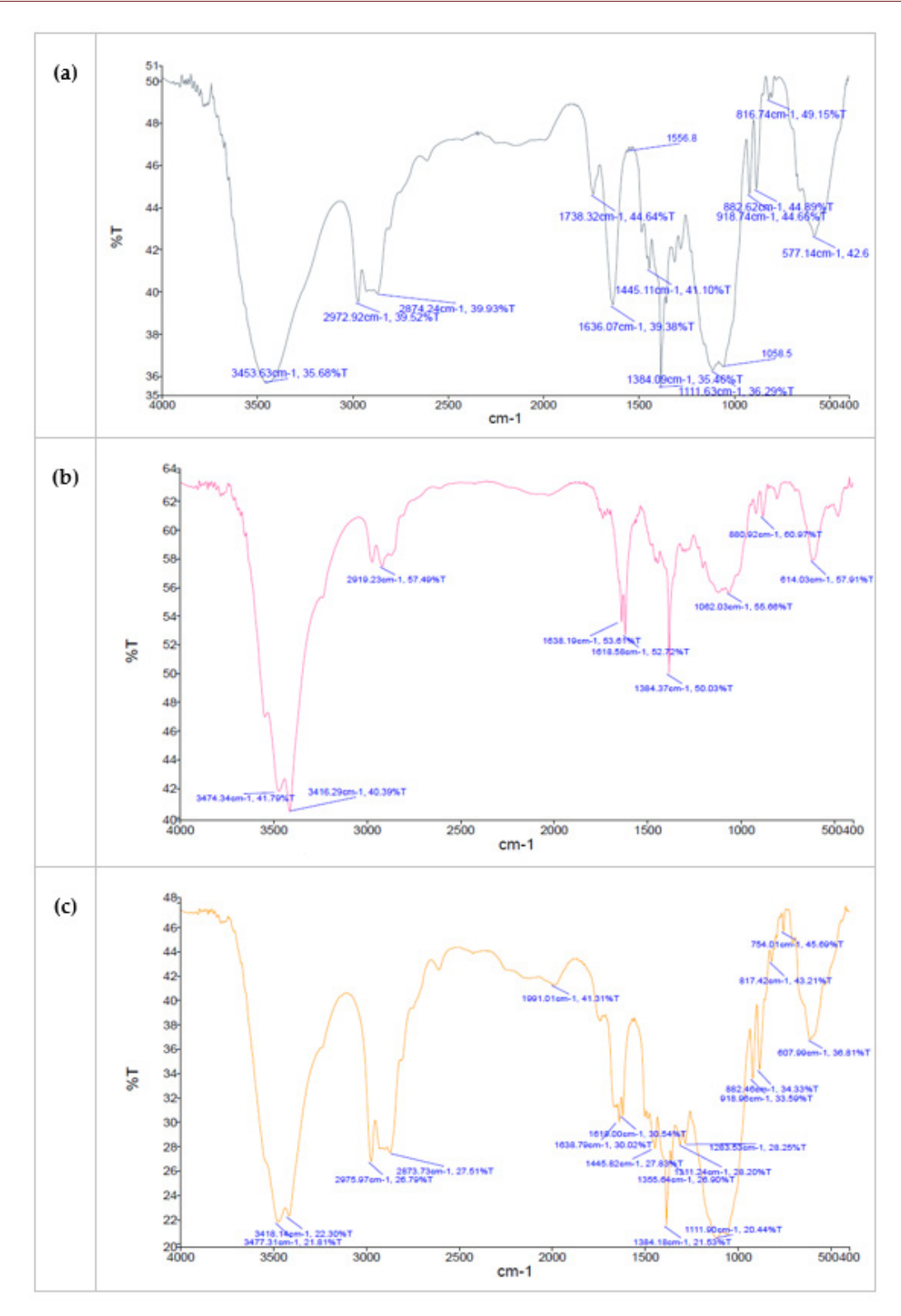


Figure 2: FTIR spectra of (a) blank nanosponges, (b) rutin loaded nanosponges, and (c) brucine loaded nanosponges.

presence in prepared nanosponges.<sup>38</sup> Further, brucine loaded nanosponges showed characteristic drug peaks at 3477/3418 cm<sup>-1</sup> (O-H stretching), 2976/2874 cm<sup>-1</sup> (C-H stretching), 1638 cm<sup>-1</sup> (C=O stretching), and 1619 cm<sup>-1</sup> (aromatic stretching), confirming the drug presence in the formulation.<sup>39,40</sup> The

spectra confirm the presence of both drugs, ethyl cellulose and PVA. Overall, the absence of any new diagnostic peaks along with a very few minor shifts of some peaks here indicates drug encapsulation with no drug-excipient interaction, as described in the literature.<sup>41</sup>

#### FE-SEM

SEM has consistently been used to examine the morphology and particle size of the prepared nanosponges.<sup>33</sup> The FE-SEM micrographs of blank, rutin loaded nanosponges, and brucine loaded nanosponges are presented in Figure 3. The blank nanosponges demonstrated that the particles were discrete and non-agglomerated, with a spherical shape and surface pores with particle sizes ranging from 300 to 400 nm. The non-aggregation of nanosponges could be attributed to the inclusion of PVA in the formulation, as previously described.<sup>42</sup> On the other hand, the pore development results from the quick evaporation of organic solvent (in this case, DCM) from the surface of nanosponges.<sup>43</sup>

The rutin loaded nanosponges exhibited partial pore filling compared to blank, which could be because the bioactive was encased in the nanosponges porous architecture, according to literature.<sup>44</sup> They were spherical and possess similar particle size of blanks. The brucine loaded nanosponges displayed a similar gross morphology to the blank nanosponges. These observations were consistent with earlier studies reported.<sup>29,35</sup>

# **DSC Study**

According to the literature, DSC can be used to determine the physical state of the drug in nanosponges as well as to validate whether the guest molecules are trapped in their porous spaces.<sup>29</sup>

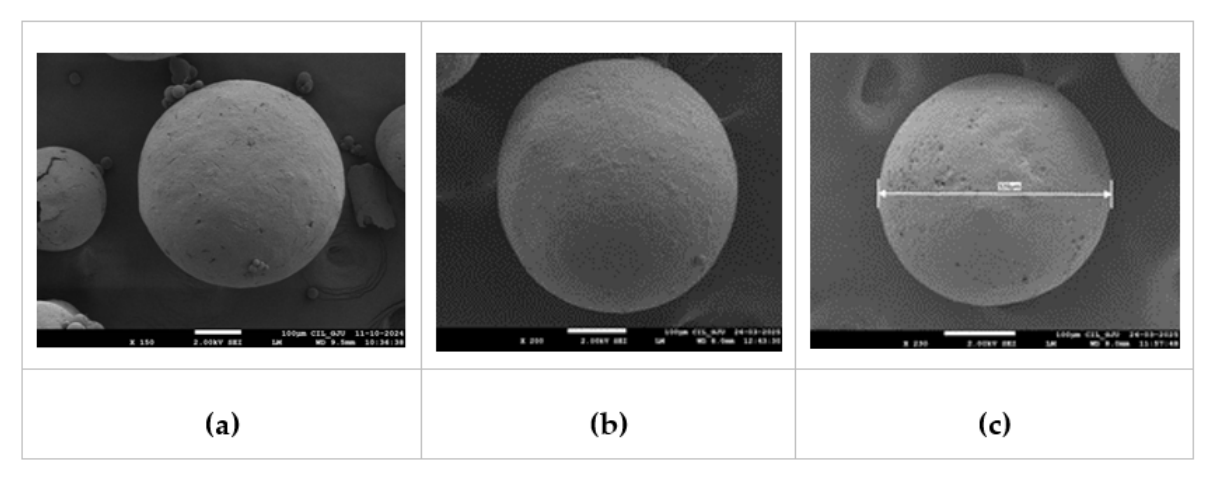


Figure 3: FESEM image of (a) blank, (b) rutin loaded nanosponges, and (c) brucine loaded nanosponges. The scale bar represents 100 μm.

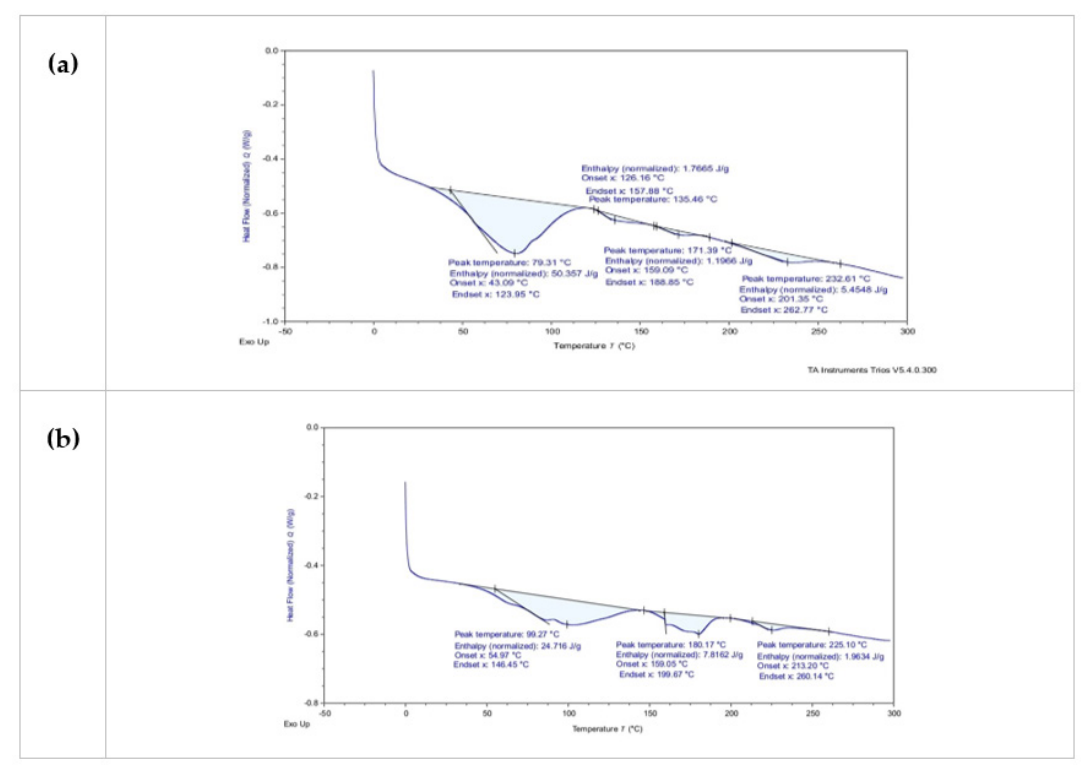


Figure 4: DSC thermogram of (a) blank nanosponges, and (b) rutin plus brucine nanosponges combination.

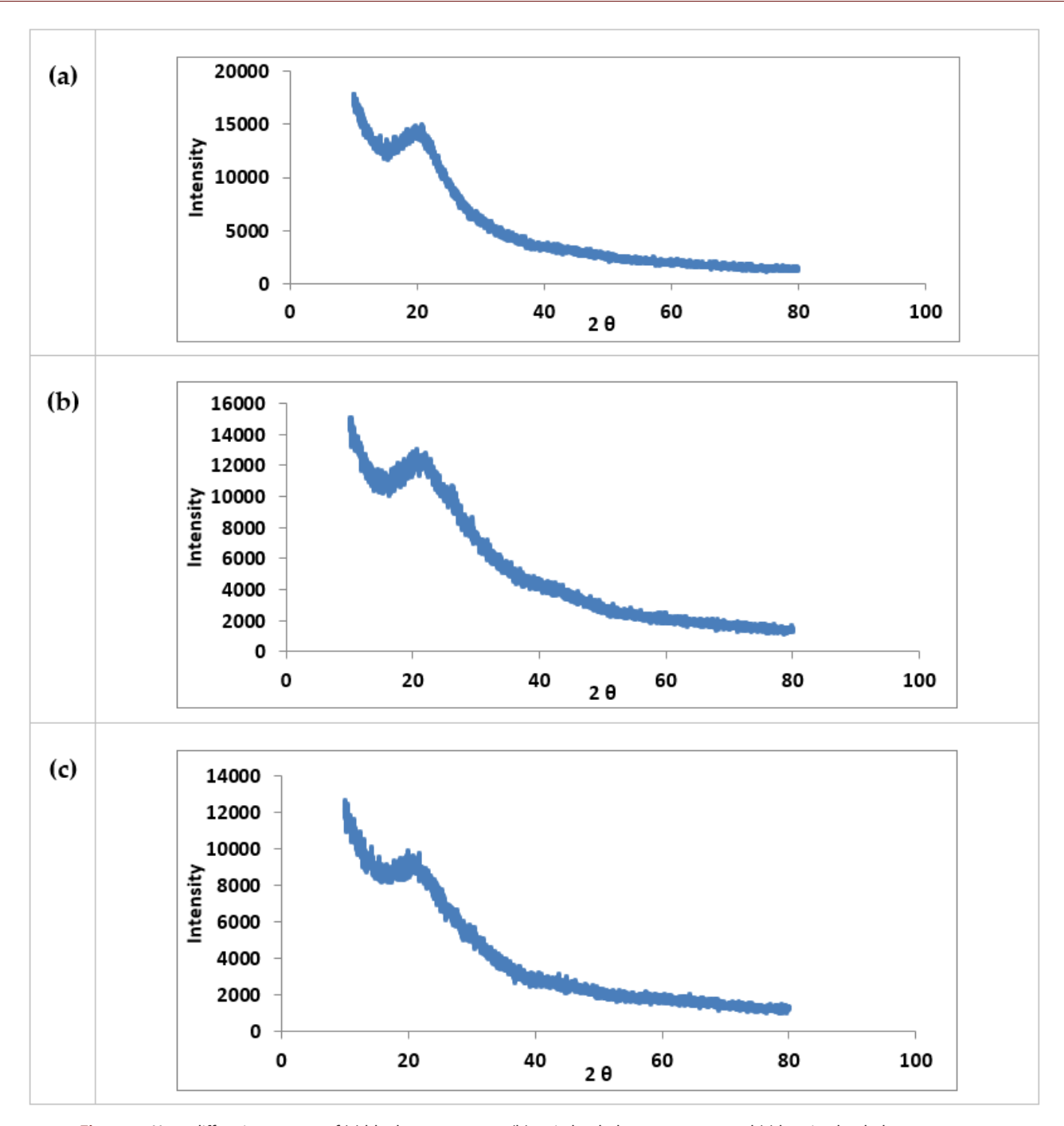


Figure 5: X-ray diffraction pattern of (a) blank nanosponges, (b) rutin loaded nanosponges, and (c) brucine loaded nanosponges.

Thermal analysis of blank, and rutin plus brucine nanosponges combination is presented in Figure 4. The blank thermogram revealed a broad exothermic peak around 45-85°C, indicating water loss during the initial heating cycle, which is typical in this temperature range. The thermal events observed at 135°C and 171°C correspond to the glass transition temperature and melting point, respectively, of ethyl cellulose. Another wide exotherm observed at 232.61°C matches to the melting point of PVA. The slight fluctuation in glass transition temperature and enthalpy reported here could be attributed to the interaction of ethyl cellulose and PVA in blank nanosponges. On the other hand, the

bioactive loaded nanosponges showed a broad low temperature event (55-146°C), probably attributed to the bound water. The minor events observed at 159-199°C and 213-260°C correspond to the brucine and rutin melting points, respectively, which also confirms the successful entrapment of bioactives in the developed nanosponges. Interestingly, the absence of any sharp peaks here suggests the bioactives are in amorphous state.

# X-ray Diffraction

XRD studies on nanosponges were generally carried out to investigate the crystallinity of pure bioactives in the samples

after their entrapment in nanosponges. 46 In the present study, XRD was performed for blank, rutin loaded, and brucine loaded nanosponges, and are presented in Figure 5. It has been reported that the crystalline properties of rutin is indicated by a sharp diffraction peak at  $2\theta=26.22^{\circ}$ . Similarly, crystalline properties of brucine was evidenced by sharp peaks at  $2\theta=11.98^{\circ}$ ,  $13.82^{\circ}$ , 18.32°, 21.44°, 22.74°, 23.79° and 32.72° according to an earlier study.<sup>47</sup> However, in the current investigation, it is evident from the diffractograms (Figure 5) that both blank nanosponges and bioactives loaded nanosponges did not show any crystalline peaks. This investigation demonstrated that the low intensity XRD diffraction peaks obtained here signifies the crystalline character of rutin/brucine was totally changed to amorphous form when encapsulated in nanosponges. Similar findings were obtained for carbamazepine nanosponges fabricated employing ethyl cellulose polymer via quasi emulsion technique.<sup>26</sup>

#### In vitro Release

The effectiveness and therapeutic potential of developed formulations are evaluated by drug release tests, which replicate the availability of drugs at the site of action. This investigation ensures the uniformity, efficacy, and compatibility of the formulation and helps predict *in vivo* behavior.<sup>48</sup> Furthermore, this test is a way to assess the quality of developed formulations. Figure 6 compares the release profiles of pure rutin, pure brucine, rutin loaded nanosponges, and brucine loaded nanosponges. The figure reveals that the release of pure rutin was comparatively slow (though being more hydrophilic than brucine) and consistent, with only ~67% in 6 hr, while it was rapid and complete with pure brucine. Two distinct release profiles were exhibited by pure rutin and rutin loaded nanosponges. Indeed, the release was considerably decreased when rutin was loaded in the nanosponges

and the cumulative amount released was statistically significant (p<0.0001). Similar observation was also noticed with brucine loaded nanosponges, with the % release at the end of the study being low (p<0.05) as compared to pure brucine. Overall, the release of bioactives from nanosponges was observed to be slower when compared to that of pure bioactives. This slower diffusion into the external medium could be attributed to the hydrophobic nature of the polymer used, which might have hindered media penetration into the nanoparticle matrix. It is well documented in the literature that nanosponges provide sustained release of entrapped bioactives encapsulated within their internal matrix. 49,50 The results of release kinetics data of pure rutin and pure brucine suggest the best-fit with the first-order release model, as evidenced by the highest regression coefficients (R<sup>2</sup>=0.9502 for rutin and 0.9790 for brucine). However, the release behavior of both bioactives loaded nanosponges displayed good fit with the zero-order model (R<sup>2</sup>=0.9402 for rutin and 0.9878 for brucine), signifying consistent drug release. Such release behavior has been reported earlier, further supporting the reliability of the present observations.51,52

# In vitro Anti-oxidant Activity

The anti-oxidant activity is based on the reduction of DPPH, which is a persistent free radical with an odd electron and produces a purple color at  $\lambda_{max}$  517, making it the most absorbent. Antioxidants serve an important role in converting DPPH into its reduced form, DPPH-H, which has a decreased absorbance when combined with hydrogen donor. This technique is critical for determining a compound's free radical scavenging capacity. The extent of decolorization from violet to yellow correlates with the number of electrons collected, indicating a higher antioxidant potential.<sup>53</sup> The antioxidant activity of

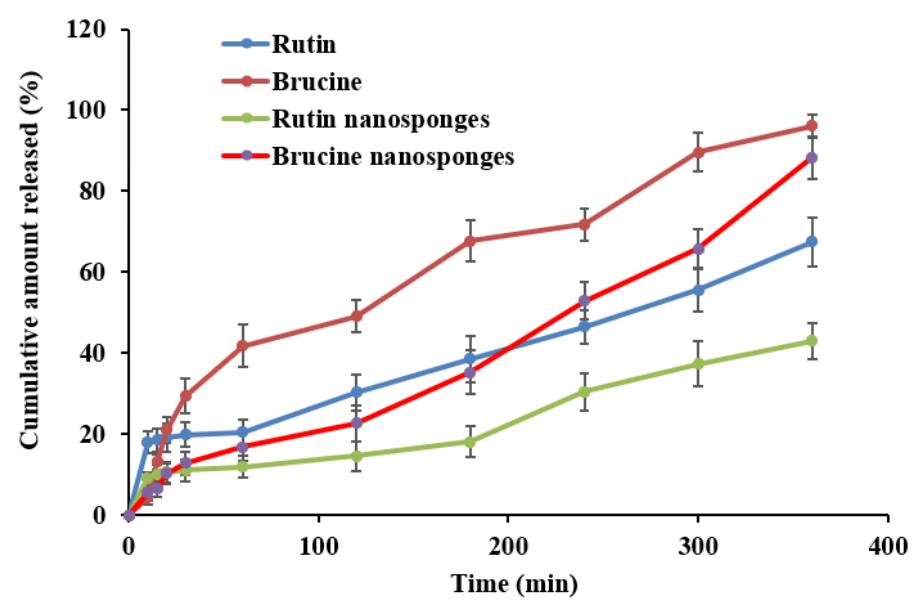


**Figure 6:** Comparative *in vitro* release profiles of pure rutin, pure brucine, rutin loaded nanosponges, and brucine loaded nanosponges.

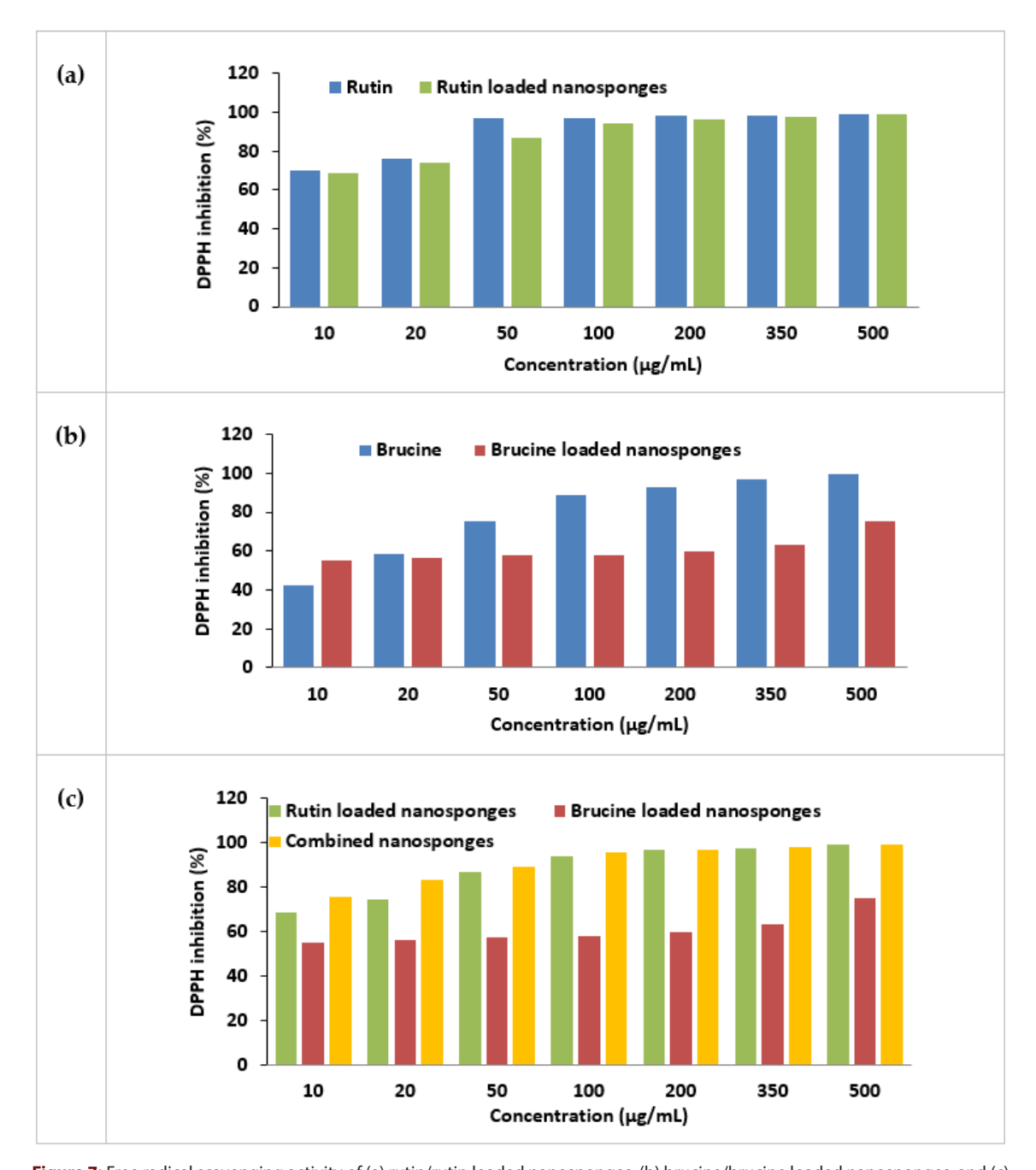


**Figure 7:** Free radical scavenging activity of (a) rutin/rutin loaded nanosponges, (b) brucine/brucine loaded nanosponges, and (c) rutin plus brucine nanosponges combination.

pure rutin, pure brucine, rutin loaded nanosponges, brucine loaded nanosponges, and combined nanosponges is presented in Figure 7. For pure rutin, the % inhibition for free radicals was found ranging from 70.10% to 99.09% (Figure 7a), which was comparable to an earlier finding.  $^{54}$  On the other hand, for rutin loaded nanosponges, the inhibition was from 68.52% to 99.00%. At lower concentrations, the activity was relatively lower than pure rutin; however, at higher concentrations (350 and 500  $\mu g/mL$ ), the inhibition was comparable. Similar to pure rutin, pure brucine showed an increase in % inhibition of free radicals when the concentration of bioactives used is increased (Figure 7). However, its antioxidant potential was found to be

lower than rutin at the same concentrations. When compared to brucine loaded nanosponges, pure brucine was found to be more effective at the same concentrations. The highest concentration of brucine loaded nanosponges tested (500  $\mu$ g/mL) showed 75.17% inhibition, which is lower than rutin and rutin nanosponges, though comparable to ascorbic acid (generally used as standard for antioxidant assay) reported in literature. <sup>55</sup>

A comparison of the antioxidant activity of pure brucine and pure rutin at a greater concentration (500  $\mu g/mL$ ) reveals a similar effectiveness; however, rutin outperformed its brucine counterpart at the lowest measured dose (10  $\mu g/mL$ ). This

may be attributed to the number as well as the location of electron-donating group (OCH<sub>3</sub> group for brucine and OH group for rutin) in the respective bioactives.<sup>56,57</sup> Brucine possesses two methoxy groups located at 9 and 10 positions of the aromatic ring,<sup>58</sup> whereas rutin has five hydroxy groups located at A ring (C-5 and C-7), B ring (C-3 and C-4), C ring (C-3).<sup>59</sup> It is worth mentioning that the type of groups and their location, along with their number have played a role in exhibiting the antioxidant effect.

It is apparent from Figure 7C that rutin loaded nanosponges showed higher DPPH scavenging than brucine loaded nanosponges across all concentrations. The 1:1 (w/w) mixture of rutin loaded nanosponges and brucine loaded nanosponges (combination) demonstrated synergetic inhibition (as brucine potentiates the effect of rutin) than rutin alone at low doses (10-50 µg/mL), and was comparable at higher levels. The increased percentage inhibition observed with the combination (half the dose of rutin and brucine) at low dose could be explained by the fact that brucine nanosponges and rutin nanosponges enhanced the scavenging effect of the combination more than individual nanosponges may be through a synergistic effect. However, at greater doses, the assay approaches an upper limit, so the combined effect is not visible.

## In vitro Cytotoxicity Assay

The MTT test, typically used to screen dose-response relationships and obtain IC50 values, was used to examine the cytotoxic response of the developed nanosponges. The HaCaT cells, which are immortalized human keratinocytes, are a valuable normal-cell comparator for evaluating off-target toxicity and were used in this work. The cytotoxicity effect of rutin loaded nanosponges, brucine loaded nanosponges, and combined nanosponges is presented in Figure 8. Three distinct curves were noticed when HaCaT cells were treated with different nanosponge formulations, and viability decreased with the tested concentration (1-1350 μg/mL). Rutin loaded and brucine loaded nanosponges had comparable IC<sub>50</sub> values (83.52 μg/mL and 79.34 μg/mL, respectively), but interestingly, combined nanosponges had a significantly lower  $IC_{50}$  of 20.66 µg/mL. This ~4 fold improvement in potency suggests that delivering these bioactives in nanosponges as a combination enhances the overall cytotoxic effect on HaCaT. The possible reasons for this additive activity could be due to the complementary mechanisms, wherein a polyphenolic flavonoid (rutin) and a strychnos alkaloid (brucine) scaffold engage distinct redox and signaling pathways.<sup>25,59</sup> According to reports, rutin inhibits the growth of certain cancer types by altering signaling pathways that control oxidative stress, apoptosis, angiogenesis, and cell cycle progression.<sup>60</sup> Similarly, brucine, a multi-target anticancer agent, inhibits angiogenesis via VEGFR-2/VEGF/

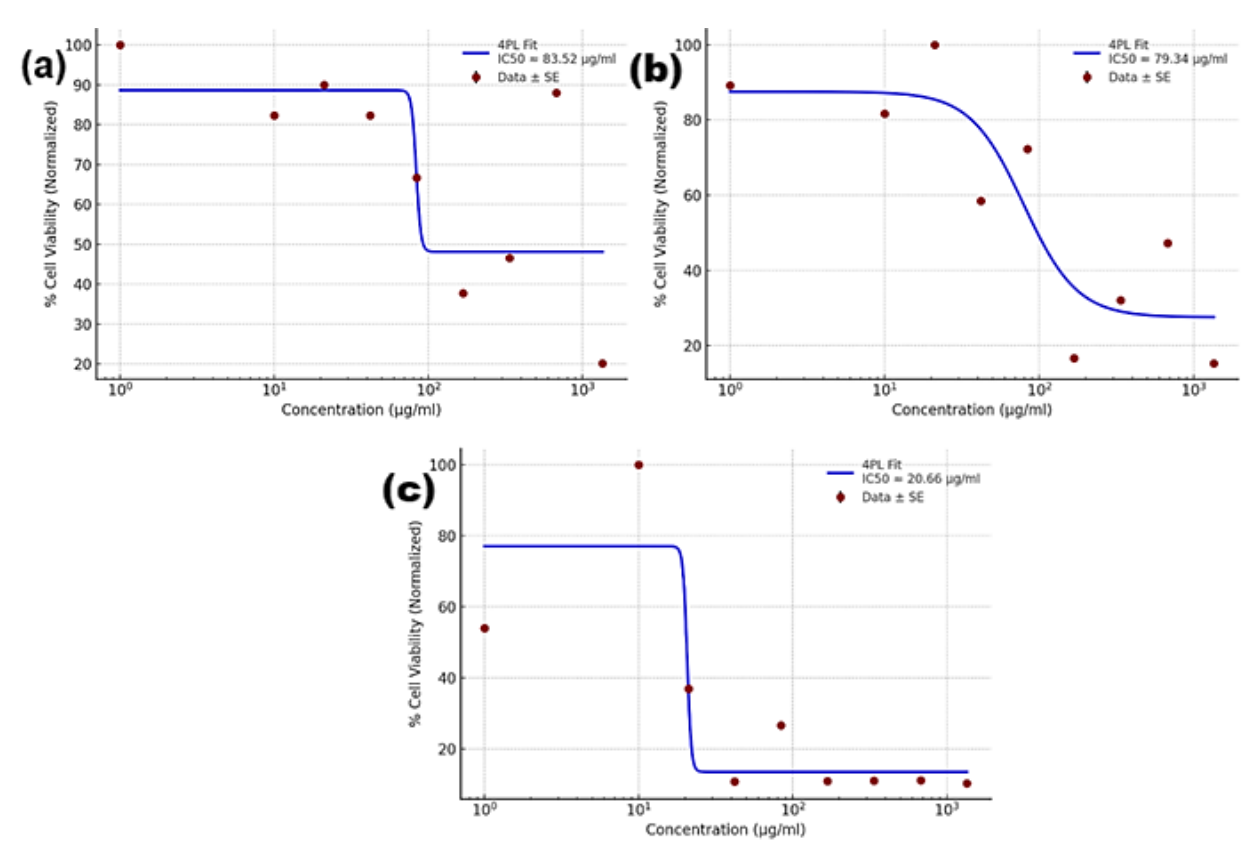


**Figure 8:** MTT viability assay results of cells treated with different concentrations of (a) rutin loaded nanosponges, (b) brucine loaded nanosponges, and (c) rutin plus brucine nanosponges combination.

TNF- $\alpha$  modulation, suppresses Wnt/ $\beta$ -catenin and HIF-1 signaling, and induces mitochondrial apoptosis, thereby limiting proliferation, migration, and invasion. Overall, the results of this study demonstrated a synergetic cytotoxic effect when the rutin loaded nanosponges and brucine loaded nanosponges are combined.

# **CONCLUSION**

The current study investigated the possibility of combination delivery of rutin and brucine nanosponges to boost therapeutic efficacy in cancer therapy. Rutin and brucine nanosponges were made separately, resulted in higher encapsulation. The FTIR spectra confirm drug encapsulation and no drug-excipient interaction. Scanning electron microscopy shows that the particles are spherical, non-aggregation, and in the nano size range. Thermal examination reveals that bioactives were successfully entrapped in the prepared nanosponges, and are in amorphous state. The X-ray diffractograms of both blank and bioactive loaded nanosponges showed no crystalline peaks. In vitro release findings demonstrated that encapsulating rutin/brucine in nanosponges considerably delayed and prolonged release as compared to pure bioactives. At low doses (10-50 µg/mL), combined delivery of nanosponges inhibited DPPH scavenging more effectively than rutin or brucine alone. Interestingly, the combination demonstrated stronger anticancer activity with a significantly lower IC<sub>50</sub> value than when utilized alone in the MTT assay.

# **ACKNOWLEDGEMENT**

The authors acknowledge the Deanship of Scientific Research, Vice-Presidency for Graduate Studies and Scientific Research, King Faisal University for the support.

# **ABBREVIATIONS**

**DCM:** Dichloromethane; **DPPH:** 2,2-diphenyl-1-picrylhydrazyl; **DSC:** Differential Scanning Calorimetry; **FE-SEM:** Field Emission- Scanning Electron Microscopy; **FTIR:** Fourier Transform Infrared; **MTT:** 3-[4,5-dimethylthiazol-2-yl]-2,5 diphenyl tetrazolium bromide; **PVA:** Polyvinyl Alcohol; **SEM:** Scanning Electron Microscopy.

#### **FUNDING**

This work was supported through the Ambitious Researcher track-Research Articles by the Deanship of Scientific Research, Vice Presidency for Graduate Studies and Scientific Research, King Faisal University, Al-Ahsa, Saudi Arabia [Grant Number KFU253850].

# **CONFLICT OF INTEREST**

The authors declare that there is no conflict of interest.

#### REFERENCES

- Hanahan D. Hallmarks of cancer: new dimensions. Cancer Discov. 2022;12(1):31-46. doi: 10.1158/2159-8290.CD-21-1059, PMID 35022204.
- Sung H, Ferlay J, Siegel RL, Laversanne M, Soerjomataram I, Jemal A, et al. Global cancer statistics 2020: GLOBOCAN estimates of incidence and mortality worldwide for 36 cancers in 185 countries. CA Cancer J Clin. 2021;71(3):209-49. doi: 10.3322/ca ac.21660, PMID 33538338.
- Ferlay J, Colombet M, Soerjomataram I, Parkin DM, Piñeros M, Znaor A, et al. Cancer statistics for the year 2020: an overview. Int J Cancer. 2021. doi: 10.1002/ijc.33588, PMID 33818764.
- Miller KD, Nogueira L, Devasia T, Mariotto AB, Yabroff KR, Jemal A, et al. Cancer treatment and survivorship statistics, 2022. CA Cancer J Clin. 2022;72(5):409-36. doi: 10.3322/caac.21731, PMID 35736631.
- Siegel RL, Miller KD, Wagle NS, Jemal A. Cancer statistics, 2023. CA Cancer J Clin. 2023;73(1):17-48. doi: 10.3322/caac.21763, PMID 36633525.
- Vasan N, Baselga J, Hyman DM. A view on drug resistance in cancer. Nature. 2019;575(7782):299-309. doi: 10.1038/s41586-019-1730-1, PMID 31723286.
- Mitchell MJ, Billingsley MM, Haley RM, Wechsler ME, Peppas NA, Langer R. Engineering precision nanoparticles for drug delivery. Nat Rev Drug Discov. 2021;20(2):101-24. doi: 10.1038/s41573-020-0090-8, PMID 33277608.
- Beck A, Goetsch L, Dumontet C, Corvaïa N. Strategies and challenges for the next generation of antibody-drug conjugates. Nat Rev Drug Discov. 2017;16(5):315-37. doi: 10.1038/nrd.2016.268, PMID 28303026.
- Kumar G, Virmani T, Sharma A, Pathak K. Codelivery of phytochemicals with conventional anticancer drugs in form of nanocarriers. Pharmaceutics. 2023;15(3):889. doi: 10.3390/pharmaceutics15030889, PMID 36986748.
- Aljabali AA, Obeid MA, Bashatwah RM, Qnais E, Gammoh O, Alqudah A, et al. Phytochemicals in cancer therapy: A structured review of mechanisms, challenges, and progress in personalized treatment. Chem Biodivers. 2025;22(8):e202402479. doi: 10.1002/cbdv.202402479, PMID 40192260.
- Rizeq B, Gupta I, Ilesanmi J, AlSafran M, Rahman MM, Ouhtit A. The power of phytochemicals combination in cancer chemoprevention. J Cancer. 2020;11(15):4521-33. doi: 10.7150/jca.34374, PMID 32489469.
- Upadhyay P, Ghosh A, Sarangthem V, Singh TD. Nanocarrier mediated co-delivery of phytochemicals and chemo-drugs: an emerging strategy to combat lung cancer in a systemic way. Phytochem Rev. 2024;23(2):485-527. doi: 10.1007/s11101-023-09894-9.
- Jacob S, Kather FS, Boddu SH, Rao R, Nair AB. Vesicular carriers for phytochemical delivery: A comprehensive review of techniques and applications. Pharmaceutics. 2025;17(4). doi: 10.3390/pharmaceutics17040464.
- Jacob S, Kather FS, Morsy MA, Boddu SH, Attimarad M, Shah J, et al. Advances in nanocarrier systems for overcoming formulation challenges of curcumin: current insights. Nanomaterials (Basel). 2024;14(8):672. doi: 10.3390/nano14080672, PMID 38668166
- Trotta F, Dianzani C, Caldera F, Mognetti B, Cavalli R. The application of nanosponges to cancer drug delivery. Expert Opin Drug Deliv. 2014;11(6):931-41. doi: 10.1517/174 25247.2014.911729, PMID 24811423.
- Dombe S, Shirote P. Nanosponges encapsulated phytochemicals for targeting cancer: a review. Curr Drug Targets. 2021;22(4):443-62. doi: 10.2174/138945012199 9201012201455, PMID 33045959.
- 17. Biharee A, Bhartiya S, Yadav A, Thareja S, Jain AK. Microsponges as drug delivery system: past, present, and future perspectives. Curr Pharm Des. 2023;29(13):1026-45. doi: 10.2174/1381612829666230404082743, PMID 37013425.
- Pushpalatha R, Selvamuthukumar S, Kilimozhi D. Cyclodextrin nanosponge based hydrogel for the transdermal co-delivery of curcumin and resveratrol: development, optimization, in vitro and ex vivo evaluation. J Drug Deliv Sci Technol. 2019;52:55-64. doi: 10.1016/j.jddst.2019.04.025.
- Hariri G, Edwards AD, Merrill TB, Greenbaum JM, van der Ende AE, Harth E. Sequential targeted delivery of paclitaxel and camptothecin using a cross-linked "nanosponge" network for lung cancer chemotherapy. Mol Pharm. 2014;11(1):265-75. doi: 10.1021 /mp400432b, PMID 24215299.
- Gholibegloo E, Mortezazadeh T, Salehian F, Forootanfar H, Firoozpour L, Foroumadi A, et al. Folic acid decorated magnetic nanosponge: an efficient nanosystem for targeted curcumin delivery and magnetic resonance imaging. J Colloid Interface Sci. 2019;556:128-39. doi: 10.1016/j.jcis.2019.08.046, PMID 31437658.
- Tannous M, Trotta F, Cavalli R. Nanosponges for combination drug therapy: state-of-the-art and future directions. Nanomedicine (London, England). 2020;15(7):643-6. doi: 10.2217/nnm-2020-0007, PMID 32077373.
- Imani A, Maleki N, Bohlouli S, Kouhsoltani M, Sharifi S, Maleki Dizaj S. Molecular mechanisms of anticancer effect of rutin. Phytother Res. 2021;35(5):2500-13. doi: 1 0.1002/ptr.6977, PMID 33295678.
- Pandey A, Kumar R, Mishra A, Pandey A, Pandey AK. Recent updates on the pharmacological potential of plant-based Rutin. Curr Nutraceuticals. 2022;3(2). doi: 1 0.2174/2665978603666220614151613.
- Kang Q, Zheng K, Jiang GM, Li YK, Liang YB, Geng Q, et al. Brucine suppresses proliferation and promotes apoptosis of human cholangiacarcinoma cells via the inhibition of COX2 expression. J Cancer. 2023;14(14):2700-6. doi: 10.7150/jca.8751 4, PMID 37779869.

- Lu L, Huang R, Wu Y, Jin JM, Chen HZ, Zhang LJ, et al. Brucine: a review of phytochemistry, pharmacology, and toxicology. Front Pharmacol. 2020;11:377. doi: 10.3389/fphar.2020.00377, PMID 32308621.
- Abdalla KF, Osman MA, Nouh AT, El Maghraby GM. Microsponges for controlled release and enhanced oral bioavailability of carbamazepine. J Drug Deliv Sci Technol. 2021;65:102683. doi: 10.1016/j.jddst.2021.102683.
- Desavathu M, Pathuri R, Chunduru M. Design, development and characterization of valsartan microsponges by quasi emulsion technique and the impact of stirring rate on microsponge formation. J App Pharm Sci. 2017;7(1):193-8. doi: 10.7324/JAPS.20 17.70128.
- Morsy MA, Nair AB. Prevention of rat liver fibrosis by selective targeting of hepatic stellate cells using hesperidin carriers. Int J Pharm. 2018;552(1-2):241-50. doi: 10.101 6/j.ijpharm.2018.10.003, PMID 30291958.
- Wadhwa G, Kumar S, Mittal V, Rao R. Encapsulation of babchi essential oil into microsponges: physicochemical properties, cytotoxic evaluation and anti-microbial activity. J Food Drug Anal. 2019;27(1):60-70. doi: 10.1016/j.jfda.2018.07.006, PMID 30648595
- 30. Kumria R, Nair AB, Al-Dhubiab BE. Loratidine buccal films for allergic rhinitis: development and evaluation. Drug Dev Ind Pharm. 2014;40(5):625-31. doi: 10.3109/03639045.2014.884125, PMID 24506459.
- Nair A, Gupta R, Vasanti S. In vitro controlled release of alfuzosin hydrochloride using HPMC-based matrix tablets and its comparison with marketed product. Pharm Dev Technol. 2007;12(6):621-5. doi: 10.1080/10837450701563277, PMID 18161635.
- Gupta B, Dalal P, Rao R. Cyclodextrin decorated nanosponges of sesamol: antioxidant, anti-tyrosinase and photostability assessment. Food Biosci. 2021;42:101098. doi: 10 .1016/j.fbio.2021.101098.
- Mahant S, Kumar S, Nanda S, Rao R. Microsponges for dermatological applications: perspectives and challenges. Asian J Pharm Sci. 2020;15(3):273-91. doi: 10.1016/j.ajp s.2019.05.004, PMID 32636947.
- 34. Srinatha N, Battu S, Vishwanath BA. Microsponges: a promising frontier for prolonged release-current perspectives and patents. Beni Suef Univ J Basic Appl Sci. 2024;13(1):60. doi: 10.1186/s43088-024-00519-4.
- Arya P, Pathak K. Assessing the viability of microsponges as gastro retentive drug delivery system of curcumin: optimization and pharmacokinetics. Int J Pharm. 2014;460(1-2):1-12. doi: 10.1016/j.ijpharm.2013.10.045, PMID 24184218.
- Giotopoulou I, Stamatis H, Barkoula NM. Encapsulation of thymol in ethyl cellulose-based microspheres and evaluation of its sustained release for food applications. Polymers. 2024;16(23):3396. doi: 10.3390/polym16233396, PMID 39684141.
- Anroop B, Ghosh B, Parcha V, Kumar A, Khanam J. Synthesis and comparative skin permeability of atenolol and propranolol esters. J Drug Deliv Sci Technol. 2005;15(2):187-90. doi: 10.1016/S1773-2247(05)50025-X.
- Naeem A, Yu C, Zang Z, Zhu W, Deng X, Guan Y. Synthesis and evaluation of rutin-hydroxypropyl β-cyclodextrin inclusion complexes embedded in xanthan gum-based (HPMC-g-AMPS) hydrogels for oral controlled drug delivery. Antioxidants (Basel, Switzerland). 2023;12(3):552. doi: 10.3390/antiox12030552, PMID 36978800.
- Elsewedy HS, Dhubiab BE, Mahdy MA, Elnahas HM. Development, optimization, and evaluation of pegylated brucine-loaded PLGA nanoparticles. Drug Deliv. 2020;27(1):1134-46. doi: 10.1080/10717544.2020.1797237, PMID 32729331.
- Anroop B, Ghosh B, Parcha V, Khanam J. Transdermal delivery of atenolol: effect of prodrugs and iontophoresis. Curr Drug Deliv. 2009;6(3):280-90. doi: 10.2174/156720 109788680895, PMID 19604142.
- 41. Kumar S, Nair AB, Kadian V, Dalal P, Jangir BL, Aldhubiab B, et al. Development and evaluation of hydrogel-based sulfasalazine-loaded nanosponges for enhanced topical psoriasis therapy. Pharmaceuticals (Basel, Switzerland). 2025;18(3):391. doi: 10.3390/ph18030391, PMID 40143167.
- Deshmukh K, Poddar SS. Tyrosinase inhibitor-loaded microsponge drug delivery system: new approach for hyperpigmentation disorders. J Microencapsul. 2012;29(6):559-68. doi: 10.3109/02652048.2012.668955, PMID 22468629.
- 43. Salah S, Awad GE, Makhlouf Al. Improved vaginal retention and enhanced antifungal activity of miconazole microsponges gel: formulation development and *in vivo*

- therapeutic efficacy in rats. Eur J Pharm Sci. 2018;114:255-66. doi: 10.1016/j.ejps.2017.12.023. PMID 29288706.
- Nair AB, Dalal P, Kadian V, Kumar S, Kapoor A, Garg M, et al. Formulation, characterization, anti-inflammatory and cytotoxicity study of sesamol-laden nanosponges. Nanomaterials (Basel, Switzerland). 2022;12(23):4211. doi: 10.3390/n ano12234211, PMID 36500833.
- Shlush E, Davidovich-Pinhas M. Influence of hot-melt extrusion and acetone-based solution casting on the characteristics of ethyl cellulose films with myvacet and glycerol mono-oleate plasticizers. Carbohydr Polym Technol Appl. 2025;10:100746. doi: 10.1016/j.carpta.2025.100746.
- Bhuptani RS, Patravale VB. Starch microsponges for enhanced retention and efficacy of topical sunscreen. Mater Sci Eng C Mater Biol Appl. 2019;104:109882. doi: 10.1016 /j.msec.2019.109882, PMID 31500041.
- 47. Kadian V, Rao R. Enhancing anti-inflammatory effect of brucine nanohydrogel using rosemary oil: a promising strategy for dermal delivery in arthritic inflammation. 3 Biotech. 2024;14(6):157. doi: 10.1007/s13205-024-03997-6, PMID 38766324.
- Shah VP, Simona Miron D, Ştefan Rădulescu F, Cardot JM, Maibach HI. In vitro release test (IVRT): principles and applications. Int J Pharm. 2022;626:122159. doi: 10.1016/j. ijpharm.2022.122159, PMID 36067919.
- Gupta S, Chopra H, Singh Bajwa P, Kumar D. Statistical formulation optimization of naproxen microsponges with Eudragit RS100 for sustained drug release. J Pharm Innov. 2025;20(4):117. doi: 10.1007/s12247-025-09994-3.
- Zheng J, Su J, Luo H, Yang W, Yu T. Innovative salicylic acid microsponges for sustained drug release. Mater Lett. 2025;382:137875. doi: 10.1016/j.matlet.2024.137875.
- 51. Bhatia M, Saini M. Formulation and evaluation of curcumin microsponges for oral and topical drug delivery. Prog Biomater. 2018;7(3):239-48. doi: 10.1007/s40204-018 -0099-9. PMID 30242738.
- Kar AK, Mahanti B, Kar B, Jana A, Chakrabarty S, Singh S, et al. Development, optimization, and in vivo bioavailability study of erlotinib hydrochloride loaded microsponge for colon targeting. Intell Pharm. 2025;3(1):1-10. doi: 10.1016/j.ipha.2 024.07.002.
- Baliyan S, Mukherjee R, Priyadarshini A, Vibhuti A, Gupta A, Pandey RP, et al. Determination of antioxidants by DPPH radical scavenging activity and quantitative phytochemical analysis of Ficus religiosa. Molecules. 2022;27(4):1326. doi: 10.3390/ molecules27041326, PMID 35209118.
- Lue BM, Nielsen NS, Jacobsen C, Hellgren L, Guo Z, Xu X. Antioxidant properties
  of modified rutin esters by DPPH, reducing power, iron chelation and human low
  density lipoprotein assays. Food Chem. 2010;123(2):221-30. doi: 10.1016/j.foodche
  m.2010.04.009.
- Khuda F, Zahir I, Khalil AA, Ali S, Ullah N, Albariqi AH, et al. Preparation, characterization, and evaluation of physcion nanoparticles for enhanced oral bioavailability: an attempt to improve its antioxidant and anticancer potential. ACS Omega. 2023;8(37):33955-65. doi: 10.1021/acsomega.3c04821, PMID 37744808.
- Chen J, Yang J, Ma L, Li J, Shahzad N, Kim CK. Author Correction: structure-antioxidant activity relationship of methoxy, phenolic hydroxyl, and carboxylic acid groups of phenolic acids. Sci Rep. 2020;10(1):5666. doi: 10.1038/s41598-020-62493-y, PMID 32205855.
- PhamTL, Ha NguyenTT, NguyenTA, Le-Deygen I, Hanh LeTM, Vu XM, et al. Antioxidant activity of an inclusion complex between rutin and β-cyclodextrin: experimental and quantum chemical studies. RSC Adv. 2024;14(26):18330-42. doi: 10.1039/d4ra02307 b. PMID 38854829.
- Jain B, Jain N, Jain S, Teja PK, Chauthe SK, Jain A. Exploring brucine alkaloid: A comprehensive review on pharmacology, therapeutic applications, toxicity, extraction and purification techniques. Phytomed Plus. 2023;3(4):100490. doi: 10.1 016/j.phyplu.2023.100490.
- Ganeshpurkar A, Saluja AK. The pharmacological potential of Rutin. Saudi Pharm J. 2017;25(2):149-64. doi: 10.1016/j.jsps.2016.04.025, PMID 28344465.
- Pandey P, Khan F, Qari HA, Oves M. Rutin (bioflavonoid) as cell signaling pathway modulator: prospects in treatment and chemoprevention. Pharmaceuticals (Basel, Switzerland). 2021;14(11):1069. doi: 10.3390/ph14111069, PMID 34832851.

Cite this article: Sardana P, Nair AB, Dalal S, Bhattacharyya MS, Jacob S, Morsy MA, et al. Investigation of Nanosponge Based Delivery of Rutin and Brucine for Cancer Therapy. Indian J of Pharmaceutical Education and Research. 2026;60(2):1-13.